

Discovery of Localized Regions of Excess 10-TeV Cosmic Rays

A. A. Abdo,¹ B. Allen,² T. Aune,³ D. Berley,⁴ E. Blaufuss,⁴ S. Casanova,⁵ C. Chen,⁶ B. L. Dingus,⁷
 R. W. Ellsworth,⁸ L. Fleysheer,⁹ R. Fleysheer,⁹ M. M. Gonzalez,¹⁰ J. A. Goodman,⁴ C. M. Hoffman,⁷
 P. H. Hütemeyer,⁷ B. E. Kolterman,⁹ C. P. Lansdell,¹¹ J. T. Linnemann,¹² J. E. McEnery,¹³ A. I. Mincer,⁹
 P. Nemethy,⁹ D. Noyes,⁴ J. Pretz,⁷ J. M. Ryan,¹⁴ P. M. Saz Parkinson,³ A. Shoup,¹⁵ G. Sinnis,⁷
 A. J. Smith,⁴ G. W. Sullivan,⁴ V. Vasileiou,⁴ G. P. Walker,⁷ D. A. Williams,³ and G. B. Yodh⁶

¹Naval Research Laboratory, Washington, DC

²Harvard-Smithsonian Center for Astrophysics, Cambridge, MA

³University of California, Santa Cruz, CA

⁴University of Maryland, College Park, MD

⁵Max Planck Institut für Kernphysik, Heidelberg, Germany

⁶University of California, Irvine, CA

⁷Los Alamos National Laboratory, Los Alamos, NM

⁸George Mason University, Fairfax, VA

⁹New York University, New York, NY

¹⁰Instituto de Astronomia, Universidad Nacional Autonoma de Mexico, D.F., MEXICO

¹¹Institute for Defense Analyses, Alexandria, VA

¹²Michigan State University, East Lansing, MI

¹³NASA Goddard Space Flight Center, Greenbelt, MD

¹⁴University of New Hampshire, Durham, NH

¹⁵Ohio State University, Lima, OH

An analysis of 7 years of Milagro data performed on a 10° angular scale has found two localized regions of excess of unknown origin with greater than 12σ significance. Both regions are inconsistent with gamma-ray emission at a level of 11σ . One of the regions has a different energy spectrum than the isotropic cosmic-ray flux at a level of 4.6σ , and it is consistent with hard spectrum protons with an exponential cutoff, with the most significant excess at ~ 10 TeV. Potential causes of these excesses are explored, but no compelling explanations are found.

PACS numbers: 95.55.Vj, 95.85.Ry, 96.50.Xy, 98.35.Eg, 98.70.Sa

Keywords: Milagro, anisotropy, cosmic rays, galactic magnetic field, heliosphere

The flux of charged cosmic rays at TeV energies is known to be nearly isotropic. This is due to Galactic magnetic fields, which randomize the directions of charged particles. However, numerous experiments across a wide range of energies have found anisotropy on large angular scales, typically with a fractional strength of $\sim 10^{-3}$ (see [1, 2, 3, 4, 5], for example). Large-scale anisotropy is also seen in data from the Milagro detector [6], but here we present the results of an analysis sensitive to intermediate angular scales ($\sim 10^\circ$).

Milagro [7] is a water Cherenkov air shower detector located in New Mexico, USA at an altitude of 2630m and at 36° N latitude. It is composed of a central 60m x 80m pond surrounded by a sparse 200m x 200m array of 175 “outrigger” water tanks. The pond is instrumented with 723 photomultiplier tubes (PMTs) in two layers. The top layer is used for event reconstruction, while the bottom layer is used to distinguish between gamma ray induced and hadron induced air showers. The outriggers, with each tank containing a single PMT, improve the angular and energy resolution of the detector for events collected after May, 2003. Milagro has a ~ 2 sr field of view, operates with a $>90\%$ duty cycle, and has a trigger rate from cosmic rays of ~ 1700 Hz, making it well-suited to searching for anisotropy in the arrival directions of

TeV cosmic rays.

For studies on small to intermediate scales ($\leq 10^\circ$), an adaptation of the point source analysis, which has been published previously [7], is suitable. A signal map is made based on the arrival direction of each event. A background map is also created using the “direct integration” technique [7], in which two-hour intervals are used to generate the background estimate. Because of this two-hour interval, the analysis is relatively insensitive to features larger than $\sim 30^\circ$ in right ascension (RA); a different analysis of the Milagro data sensitive to larger features has been performed and is presented elsewhere [6].

In the point source analysis, the signal and background maps are smoothed with a square bin of size $2.1^\circ / \cos(\delta)$ in RA by 2.1° in declination (δ), which is optimal for Milagro’s angular resolution. However, the bin size may be increased to improve the sensitivity to larger features, with a practical limit of about 10° for $\delta < 60^\circ$ (for $\delta > 60^\circ$, the RA bin width $10^\circ / \cos(\delta)$ becomes too large for the 30° background interval). The significance is calculated using the method of Li and Ma [8].

The analysis has been applied to data collected between July 2000 and August 2007. Events were required to have a zenith angle $< 45^\circ$ and $n\text{Fit} \geq 20$, where

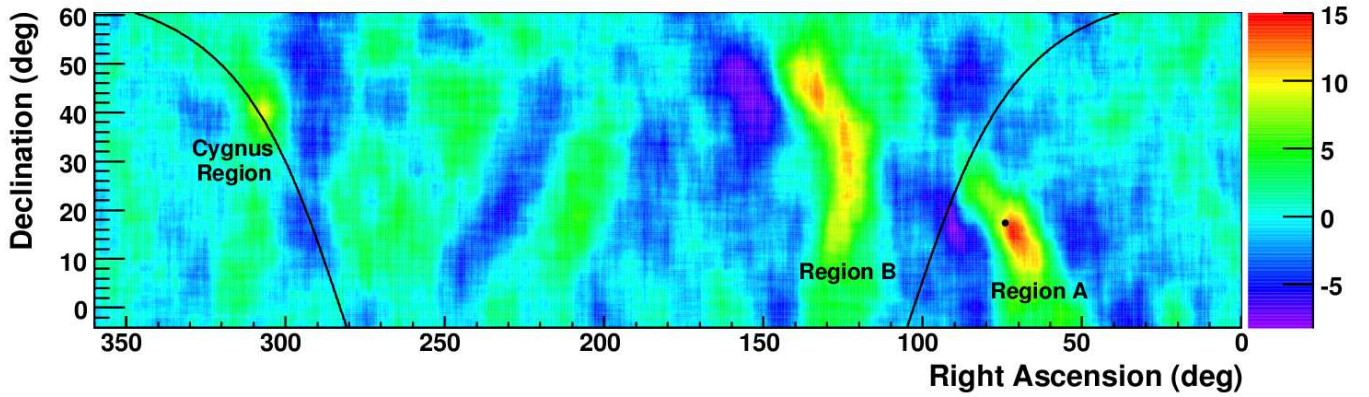


FIG. 1: Map of significances with no gamma/hadron discrimination cut and 10° binning. The color scale gives the significance, and the solid line marks the Galactic plane. The black dot marks the direction of the heliotail, which is the direction opposite the motion of the solar system with respect to the local interstellar matter. The fractional excess of Region A is $\sim 6 \times 10^{-4}$, while for Region B it is $\sim 4 \times 10^{-4}$. The deep deficits bordering the regions of excess appear because the background estimate has been raised by the excess.

nFit is the number of PMTs used in the angle fit. With these cuts, the dataset consists of 2.2×10^{11} events with a median energy of ~ 1 TeV and an average angular resolution of $< 1^\circ$. Figure 1 shows the map of significances made with 10° binning and no cuts to discriminate gamma rays from charged cosmic rays. The Cygnus Region, which has previously been shown to emit TeV gamma rays [9], is clearly visible. The excesses labeled “Region A” and “Region B” are seen with peak significances of 15.0σ and 12.7σ , respectively. While these are pre-trial significances, the excesses are great enough to remain highly significant after trials are taken into account. The fractional excess relative to the cosmic-ray background is $\sim 6 \times 10^{-4}$ for Region A and $\sim 4 \times 10^{-4}$ for Region B. Note that both excesses are paralleled by regions of deep deficit, but this is a known effect of the analysis because Regions A and B are included in the background estimate of neighboring areas in RA. Thus, the excess raises the background estimate above what it should be, resulting in a deficit.

Similarity is seen between the map in Figure 1 and results from the Tibet AS γ collaboration [2], particularly for Region A, but a direct comparison cannot be made because the analysis methods differ. For each band in δ , the Tibet analysis measured the excess (or deficit) relative to the average for that δ band, making it sensitive to the large-scale anisotropy discussed in their paper. Smaller features, such as Regions A and B, were superimposed on the large-scale variation, which is several times greater in amplitude. Conversely, in the analysis presented here, the excess/deficit was measured with respect to the local background estimate (which comes from $\pm 30^\circ$ in RA). This is illustrated in Figure 2, which shows the signal and background versus RA for a 10° band in declination. Large-scale variation dominates the figure, but the

background estimate makes the analysis sensitive only to features with an extent smaller than $\sim 30^\circ$ in RA.

To estimate the extent of Region A, an elliptical Gaussian was fit to the excess. The fit, which accounted for the change in sensitivity with declination, returned a centroid of $RA = 69.4^\circ \pm 0.7^\circ$, $\delta = 13.8^\circ \pm 0.7^\circ$, a half width of $2.6^\circ \pm 0.3^\circ$, a half length of $7.6^\circ \pm 1.1^\circ$, and an angle of $46^\circ \pm 4^\circ$ with respect to the RA axis. It is important to note that this fit focused on a “hot spot” in the general excess of Region A, but there is still excess extending to lower declinations. A fit was not performed to the excess in Region B due to its large, irregular shape.

While the excesses in Regions A and B are statistically significant, systematic causes must be ruled out. Potential weather-related effects were explored by dividing the data into the four seasons, and both excesses were seen in each season. The data were also divided into yearly datasets to investigate whether changes to the detector could play a role, and again the excesses were found in each dataset. The analysis was also run using universal time instead of sidereal time to check for day/night effects which could masquerade as a signal. In addition, the data were analyzed using anti-sidereal time, which provides a sanity check on the analysis since it will scramble real celestial features. Neither excess appears in either analysis.

The background calculation was also investigated. Figure 2 shows the number of events versus RA for the signal and background for $10^\circ < \delta < 20^\circ$, using independent 10° δ by 1° RA bins. The data for this figure were chosen to achieve an approximately uniform exposure versus RA, and the broad deficit seen by the Tibet Air Shower Array is evident (centered around $RA = 180^\circ$). As can be seen, the background is well fit, and the excess corresponding to Region A is clearly inherent in the signal. A

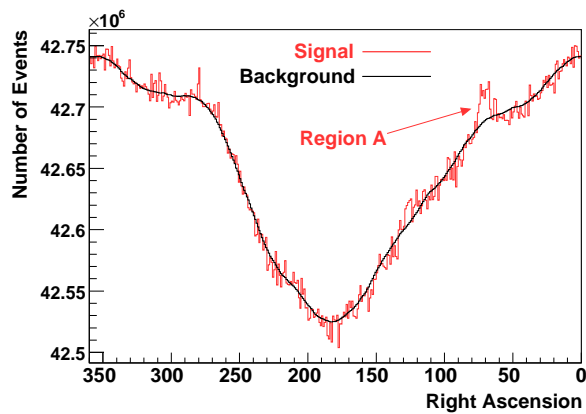


FIG. 2: Signal and background events vs RA for $10^\circ < \delta < 20^\circ$. The plot was made using independent $10^\circ \delta$ by 1° RA bins, and the data were chosen so that the exposure versus RA is approximately uniform. Region A corresponds to the excess at $RA \approx 70^\circ$. This plot shows that Region A is not due to an underestimation of the background.

similar result is found for Region B.

Diagnostic tests have been performed to gain insight into the nature of Regions A and B. For the purposes of these tests, Region A is defined as the box bounded by $66^\circ < RA < 76^\circ$ and $10^\circ < \delta < 20^\circ$. Region B is defined as the union of two boxes: $117^\circ < RA < 131^\circ$ and $15^\circ < \delta < 40^\circ$, and $131^\circ < RA < 141^\circ$ and $40^\circ < \delta < 50^\circ$. These definitions were chosen by visual inspection.

To check for flux variation, the analysis was applied to yearly and seasonal datasets. For each region, the yearly excess was consistent with a constant flux. Both regions also had a significant excess during each of the four seasons, but in both cases the fractional excess was lowest in the summer and highest in the winter. The χ^2 probability relative to a constant fractional excess was found to be about 5% for each region. While this may provide insight into the cause of these excesses, note that the χ^2 calculation considered statistical errors only, but there could be systematic effects related to weather changes.

The excesses in Regions A and B are inconsistent with gamma-ray emission. This is shown by an analysis using the compactness parameter [7], which is a gamma/hadron discriminator, and the fraction of outriggers hit in an event (f_{out}), which is correlated with energy. For the f_{out} analysis, only data with the outriggers were used, while the compactness analysis used the full dataset. As shown in Figure 3, the compactness distribution for both regions is flat compared to the Crab Nebula, which is a gamma-ray source. A flat compactness distribution could result from a very soft gamma-ray spectrum, but by considering the f_{out} distribution as well, the excess in each region is found to be inconsistent with gamma rays (and therefore electrons) at the level of 11σ .

Moreover, the energy spectrum of Region A is differ-

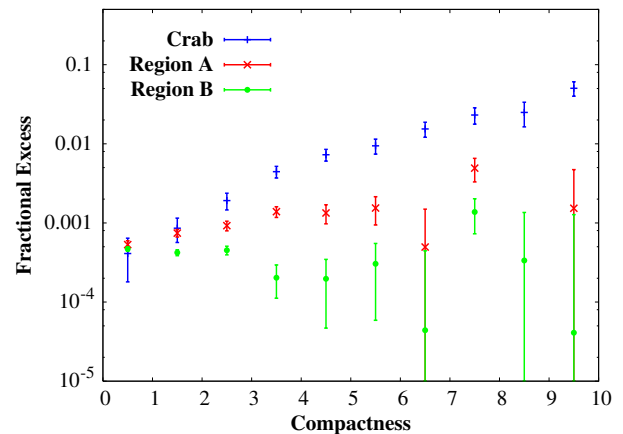


FIG. 3: Differential plot of the fractional excess versus Compactness for Regions A and B. The Crab Nebula is included to show the distribution for a gamma-ray source. The Compactness distributions, combined with the f_{out} distributions, show that both regions are inconsistent with gamma-ray emission at the 11σ level.

ent than the background, as can be seen in Figure 4a, which shows the distribution of the fractional excess versus $\log_e(f_{out})$ for both regions. If the excess had the same spectral shape as the isotropic cosmic-ray flux, the distribution would be consistent with a horizontal line. A χ^2 test of this hypothesis for Region A (B) returns a chance probability of 2×10^{-6} (6×10^{-3}). The excess of Region A is most significantly detected for $\log_e(f_{out}) \sim -1.5$, which corresponds to an energy of about 10 TeV for protons, as shown in Figure 4b. The excess can be modeled as protons with a power law spectrum with an exponential cutoff, with the best fit corresponding to a differential particle spectrum $dN/dE = E^{-1.45} e^{-E/9 \text{ TeV}}$. The range of acceptable parameters is such that the spectral index is approximately linearly correlated with the logarithm of the cutoff energy, with the 1σ range spanning from -1.9 to -0.5 for the spectral index and 4.5 TeV to 18 TeV for the cutoff energy. In addition, there is a systematic uncertainty in the spectral index of ± 0.2 due to variation in the trigger threshold, which is caused by such things as changes in atmospheric pressure or ice on the pond. There is also a 30% systematic uncertainty in the energy scale due to the threshold variation, as well as discrepancy between the simulated and measured trigger rates.

There is currently no compelling explanation for the excesses in Regions A and B. One possibility is that they could be due to neutrons, but this is unlikely because the decay length of 10 TeV neutrons is only about 0.1 parsecs, which is much closer than the nearest star. Another possibility is that these excesses could be caused by a Galactic cosmic-ray accelerator, but this is difficult because the gyroradius of a 10 TeV proton in a $2\mu\text{G}$ magnetic field, which is the estimated strength of the local

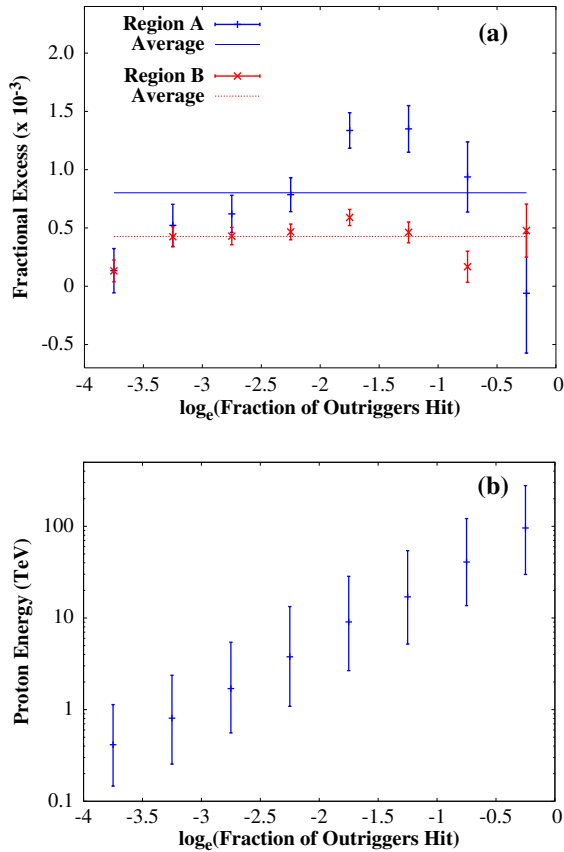


FIG. 4: (a): Differential plot of the fractional excess versus $\log_e(f_{out})$ for Regions A and B, where f_{out} is the fraction of the outriggers hit. The spectrum of Region A is significantly different than the background (2×10^{-6}), which is shown by the horizontal line. (b): Average simulated energy of protons for the $\log_e(f_{out})$ bins shown in the top plot. The error bars are asymmetric and contain the inner 68% of simulated events (i.e. the extreme 16% above and below are excluded).

Galactic field [10], is only ~ 0.005 parsecs. In order for protons from a cosmic-ray accelerator to reach us, the intervening magnetic field must connect us to the source and be coherent out to ~ 100 parsecs since there are likely no sources within this distance. However, the direction of both regions is nearly perpendicular to the expected Galactic magnetic field direction [10].

Another possibility is that one or both of the excesses could be caused by the heliosphere. This explanation is supported by the coincidence of Region A with the direction of the heliotail ($RA \approx 74^\circ$, $\delta \approx 17^\circ$ [11]), which

is the direction opposite the motion of the solar system with respect to the local interstellar matter. However, this would require either acceleration in the heliotail or shielding by the rest of the heliosphere, both of which are difficult at TeV energies.

In summary, Milagro has observed two unexplained regions of excess with high significance. Potential systematic causes have been examined and excluded. Both excesses are inconsistent with gamma rays with high confidence, and their energy spectra are moderately to strongly inconsistent with the spectrum of the isotropic cosmic-ray flux. In particular, the excess in Region A can be modeled as hard spectrum protons with a cutoff. Because there is no obvious explanation for the cause of these excesses, further observation and theoretical modeling are needed.

We gratefully acknowledge Scott Delay and Michael Schneider for their dedicated efforts in the construction and maintenance of the Milagro experiment. This work has been supported by the National Science Foundation (under grants PHY-0245234, -0302000, -0400424, -0504201, -0601080, and ATM-0002744), the US Department of Energy (Office of High-Energy Physics and Office of Nuclear Physics), Los Alamos National Laboratory, the University of California, and the Institute of Geophysics and Planetary Physics.

-
- [1] M. Ambrosio et al., Physical Review D **67**, 042002 (2003).
 - [2] M. Amenomori et al., Science **314**, 439 (2006), astro-ph/0610671.
 - [3] D. L. Hall et al., Journal of Geophysical Research **104**, 6737 (1999).
 - [4] K. Munakata et al., Physical Review D **56**, 23 (1997).
 - [5] K. Nagashima, K. Fujimoto, and R. M. Jacklyn, Journal of Geophysical Research **103**, 17429 (1998).
 - [6] B. E. Kolterman et al., 30th ICRC, Merida, Mexico (2007).
 - [7] R. Atkins et al. (Milagro), Astrophys. J. **595**, 803 (2003), astro-ph/0305308.
 - [8] T. P. Li and Y. Q. Ma, The Astrophysical Journal **272**, 317 (1983).
 - [9] A. A. Abdo et al., Astrophys. J. **658**, L33 (2007), astro-ph/0611691.
 - [10] J. L. Han, R. N. Manchester, A. G. Lyne, G. J. Qiao, and W. van Straten, Astrophys. J. **642**, 868 (2006), astro-ph/0601357.
 - [11] M. Witte, M. Banaszekiewicz, H. Rosenbauer, and D. McMullin, Advances in Space Research **34**, 61 (2004).